INL/CON-20-58881-Revision-0

Fission Product Diffusion in Silicon Carbide: As Revealed by Computer Simulations and Experimental Measurements

June 2020

Fei Gao, Isabella J Van Rooyen, William F Skerjanc, Nanjun Checn, Zhijie Jiao

Changing the World's Energy Future

Idaho National Laboratory

INL is a U.S. Department of Energy National Laboratory operated by Battelle Energy Alliance, LLC

INL/CON-20-58881-Revision-0

Fission Product Diffusion in Silicon Carbide: As Revealed by Computer Simulations and Experimental Measurements

Fei Gao, Isabella J Van Rooyen, William F Skerjanc, Nanjun Checn, Zhijie Jiao

June 2020

Idaho National Laboratory
Idaho Falls, Idaho 83415

http://www.inl.gov

Prepared for the
U.S. Department of Energy
Under DOE Idaho Operations Office
Contract DE-AC07-05ID14517

Proceedings of HTR 2020
Yogyakarta, Indonesia, October 6-8, 2020
Paper 1 HTR 2020

Fission-Product Diffusion in Silicon Carbide: As Revealed by Computer Simulations and Experimental Measurements

Fei Gao[1], Nanjun Chen[1], Zhijie Jiao[1], Isabella J. van Rooyen[2], William F. Skerjanc[3]

[1]*Nuclear Engineering and Radiological Sciences, University of Michigan, Ann Arbor, MI 48109, U.S.A*

[2]*Fuel Design and Development Department, Idaho National Laboratory, Idaho Falls, ID 83415-6188, U.S.A*

[3]*Reactor Physics Design and Analysis Department, Idaho National Laboratory, Idaho Falls, ID 83415-6188, USA*

Abstract—*The diffusion and release of fission products through silicon carbide in the tri-structural isotropic (TRISO) fuel particles remain unsolved for decades. Determining the underlying mechanism is quite challenging. To help unveil the mystery, the current work applies a molecular dynamics method to show the stability of silver, palladium, ruthenium, and iodine as interstitials and their atomic diffusion along coincident site lattice (CSL) boundaries, especially the ∑3 grain boundary (GB). The major finding describes a much faster diffusion along GB than in bulk for all elements considered. The reasonably close estimate to experiments and simulations where available has confirmed the important role of GB diffusion of Ag and Pd in SiC. However, the discrepancy addressed in Ag with measurements from fuel studies suggest a more complicated mechanism, which might be in correlation with high-energy GBs or the presence of crack. The subsequent characterization of Ru and I distribution in SiC-PyC-SiC diffusion couples, which have been ion irradiated at 900°C to 10 and 20 dpa, was performed by secondary ion mass spectrometry (SIMS) analysis. The experiment measurements correlate well with the GB diffusion by simulation, which provide further evidences that the GB diffusion cannot be neglected once fission products are accessible at the grain boundary.*

I. INTRODUCTION

Silicon carbide has unique capability in the applications of nuclear fuel due to its exceptional characteristics: high melting temperature and high thermal conductivity. The cubic polytype of SiC (3C -SiC) is believed to be most stable below 2100°C, and this has been widely explored for structural applications in nuclear reactors [1]. In high-temperature gas-cooled reactors (HTGRs), SiC is one of the constituent materials in tri-structural isotropic (TRISO) fuel particles, which has considered as a major barrier for the release of fission products (FPs), as well as providing structural support. While TRISO fuel has demonstrated excellent retention of a majority of FPs and radioisotopes, release of some metallic FPs, i.e. Ag, Pd, Ru and I, from intact fuel can still be observed in experiments under conditions similar to accident scenarios[2]. The release of FPs raises serious concern on the safety and operation of HTGRs.

Therefore, a full understanding of the transport mechanisms of FPs through 3C-SiC is required, not only to determine how it occurs so that mitigation measures can be devised, but also to support fuel performance codes[3] and provide for more-accurate fuel-behavior modeling in both normal and off-normal operating conditions. To this end, several experiments [4–10] and simulations [11–16] were performed over the past decades to investigate FP's transport through SiC. However, despite numerous experimental studies on FP transport, the microscopic mechanism governing the interactions of FPs with the fuel particle remains unclear. Hence, to identify the mechanism that contributes to transport requires information which can only be obtained by atomistic simulation.

Grain boundaries (GBs) are important for high-diffusivity paths along which diffusion can occur much faster than bulk diffusion. Their open structure along with the disruption in bonding can raise both the mobility and local thermodynamic solubility of FP through segregation. Thus, we use the molecular dynamics (MD) method to first determine FP interaction with grain boundaries in SiC. Special GBs in SiC that are most observed from TRISO fuel particles irradiated in the Advanced Gas Reactor (AGR)-1 experiment [17] are of interest. The GB characterization conducted by Kirchhofer et al. [18] has shown a high fraction of coincident-site-lattice (CSL) boundary with $\Sigma 3$ GB being dominant. Experimental research by Lillo and van Rooyen [31] on neutron irradiated TRISO coated particles identified that up to 20% Pd, Ag, and U containing precipitates are located on CSL GBs. The simulation has carried out along $\Sigma 3$ GB to provide guidance in the study of GB diffusion kinetics.

II. APPROACH

2.1 Grain Boundary Atomic Configuration

GBs were constructed by using the molecular dynamics method, which is performed by LAMMPS software package [19]. The analytical bonded order potential (ABOP) was applied to the simulations with parametrization for FP-SiC as implemented by previous work [16]. The model has an orthorhombic cell with periodic boundary conditions (PBCs) applied in directions parallel to the boundary plane. A cell consisting of two grains was used to obtain equilibrium 0K GB structure and excess energy. Within the cell, there are two crystallographically identical GBs; one is in the middle of the cell, and another periodic GB is at the upper and lower ends of the cell. There are no fixed regions of atoms within the cell, and this allows the crystal lattice to translate during energy minimization if such a translation is energetically favorable.

The basic process of determining the GB follows the same method described by Tschopp et al. [20]. First, based on the CSL theory, two differently oriented grains were brought together to obtain a bicrystal. Then, the two grains were translated rigidly with respect to each other, followed by an atom deletion process to avoid atom overlapping. The conjugate gradient (CG) algorithm was subsequently used for energy minimization. The length in the direction parallel to the tilt axis is set to be large enough (>10 nm) to avoid the interactions of GB with surfaces. The constructed $\Sigma 3$ GB lies in $(21\bar{1})$ crystallographic plane with a tilt axis in $[01\bar{1}]$ direction. The size of the CSL unit cell is 7.55 Å and 3.08 Å along [111] and $[01\bar{1}]$, respectively. The cross-section of the most stable structure of $\Sigma 3$ has been shown in Figure 1. Within the GB, there are three types of rings, containing five, seven, and six atoms, which are labeled I, II, and III, respectively. This structural feature is consistent with both transmission electron microscopy (TEM) observations [21–23] and other simulations [11], [24]. These rings can be extended to four distinct pores, with Region III being specified in upper and lower grain as IIIU and IIIL, respectively. The fourth core noted as IV was also included as a bulk-like site.

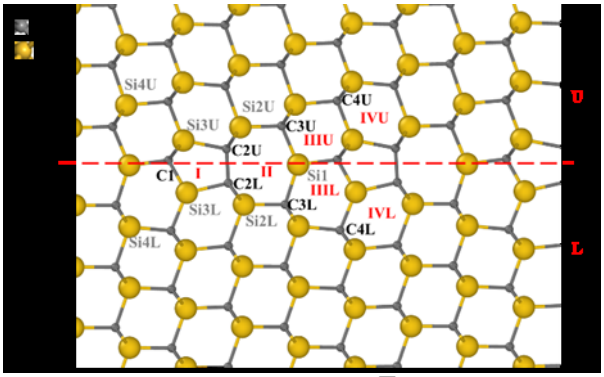

Figure 1. Bicrystal GB model of $\Sigma 3$ <110> {211} GB (gray spheres stand for carbon and yellow spheres indicate silicon). The dashed line corresponds to the GB plane separating upper (U) and lower (L) grains.

The defect formation energy associated with FPs on the distinctive GB sites can be an important term to explore with respect to diffusion kinetics. The formation energy of FP-related point defects can be defined as follow:

Here, E_{defect} is the total energy of the simulation block containing a point defect. $E_{perfect}$ stands for the total energy of a perfect cell without a defect. The integer indicates the number of atoms of type X added to (or removed from (the cell. The μ_X (X = Si or C) is the corresponding atomic chemical potential describing the exchange of particles with the respective reservoir.

2.2 Diffusion Coefficient Calculation

The diffusion kinetics of FPs along the GB were obtained by MD method with number-volume-temperature (NVT) ensemble. The temperature performed is in a range from 1200 to 3000 K. Each simulation was allowed at least 6 ns to identify the defect motion. Before the dynamic run, the atomic configurations before and after inserting the defect were relaxed for 20 ps under number-pressure-temperature (NPT) ensemble to release inner stress due to the thermal expansion for the corresponding temperature. The obtained stable configuration was then introduced to GB-diffusion study. The way to simulate the migration was described in detail elsewhere[16]. The trajectory of defect was traced during MD simulations, and the positions of all

atoms at time t are recorded. The lowest energy configurations of an FP atom at the GBs, which were relaxed to remove inner stress at a certain temperature, were used as the initial configurations for evaluating the mean-square displacements (MSDs) during the diffusion of FPs. Therefore, the diffusion coefficient can be determined by the Einstein relation from random walk theory:

where . N is the total atomic number.

Within the nuclear reactor, two environmental variables could control diffusion: temperature and radiation. On the one hand, diffusion could be a purely thermal process in which the magnitude increases with temperature. On the other hand, radiation can affect diffusion by producing additional defects that will accelerate the diffusion of atoms. To systematically investigate FP diffusion mechanisms, the diffusion coefficients as a function of temperature should be determined under various conditions (i.e., pure thermal and irradiation conditions). Pre-factors (, and activation energies () for grain boundary diffusion to calculate diffusion coefficients follow an Arrhenius relationship:

The direct output from MD simulation assumes a defect to be present 100% of the time within the cell. However, under the thermal condition, FP diffusion as a specific defect cannot exist 100% of the time. The effective diffusion coefficient can be affected by the fraction of time the defect is present or concentration ratio[12]. The effective diffusion coefficient in the realistic scenario includes both the intrinsic diffusion known here as D(T) from MD simulation and the concentration ratio, which can be described by

The concentration of the defect, *c*(def), can be determined by its formation energy along with the temperature-independent pre-factor. Since the pre-factor is able to be canceled in the concentration ratio, the relative concentration of defect can be presented by an Arrhenius form . The sum of the FP defect concentrations is contributed by the summation of all the possible FP defects that could be created. Therefore, the effective diffusion can be defined as a function of effective migration energy (and effective pre-factor (:

2.3 Experimental Detail

A novel design of multi-layer diffusion couple, reported by Dwaraknath et al. [25], was used in the experiments. The diffusion couples are ultra-high-purity 1×1 cm^2 3C-SiC plate substrates that are 0.6 mm thick. The substrates are sources from Rohm and Haas, Inc., and are coated with a thin layer of pyrocarbon and then a thin SiC cap. The fission products (Ru and I) are implanted into the PyC layer at 400 keV to a total fluence of 10^{16} cm^{-2}. The samples were then used for ion irradiations performed by a 3MV Pelletron accelerator at the University of Michigan Ion Beam Laboratory (MIBL). Total doses of 10 and 20 dpa were reached using 9MeV Si++ ions at 900°C with a dose rate of 4.610^{-4} dpa/s. Subsequently, the FPs' transport through SiC were analyzed via secondary ion mass spectrometry (SIMS). These experiments demonstrate the capability of FP diffusion into SiC substrate. The Harrison model for grain boundary and bulk diffusion was used, and an improved Whipple solution was applied to calculate the diffusion coefficients [26], [27] with details described elsewhere[28].

III. RESULTS AND DISCUSSION

3.1 *Stability of Defect in Grain Boundaries*

FP diffusion along the GB is closely related to defect formation. Therefore, FP-related point defects have been investigated in this study, including substitutional defects and interstitials. All the formation energies of FP-related point defects were calculated based on Eq. 1. Along ∑3 grain boundary, FPs can be formed on the possible vacant sites as indicated in Figure 1. In Table 1, the formation energies of FPs at the defect sites along the asymmetric GB are compared to the corresponding values in bulk[16]. To clarify our nomenclature, IIIL and IIILa denote two distinct interstitial sites formed in pore IIIL along the [01] direction. The same description applies to pore IVL, as well. When Ag is placed at the GB, the sites within channel IVL require the highest energies (> 9 eV) to form Ag interstitial. As is expected, interstitial at site IVL and IVLa, which are outside the predefined GB region with the most bulk-like structure as compared with other locations, have the closest values to that of the interstitial in bulk. The similar finding also applies to the substitutional defects when Ag occupies the atom site in Ring IV. Among the interstitials, Ag at Site IIILa was found to be the most stable configuration, with a formation energy of 5.77 eV. The energy order has been well maintained as compared with the *ab initio* calculation [11].

Following by the same trend, the Pd, Ru, and I point defects were also calculated, and adhered in Table 1. Palladium was found to be stable on a carbon-vacant site along the GB, rather than a silicon-vacant site. This is evidenced by the formation and penetration of palladium silicides along the SiC GB [29]. The most stable Pd interstitial is formed on IIILa site with the formation

energy of 5.11 eV. We found the formation energy can be significantly influenced by distinct sites along [01] direction. The difference is maximized in IIIL pore, which can reach at 2 eV. The discrepancy in formation energy along the [01] direction may be due to the formation of a Si dimer. When the atom is close to the Si dimer, the formation energy is usually higher. Along ∑3 GB, the Ru as an interstitial is likely to be stable in Pore II, with an energy of 1.20 eV, being the lowest. This is even more stable than the substitutions, which is similar to Ag.

Moreover, the overall formation energy of iodine along grain boundary is generally much higher than the other three elements, which might be due to its large atomic size and mass. The energy required to stabilize iodine as an interstitial is two to three times amount of the substitutions, which means that if a vacant site is presented, the iodine atom will most likely occupy the lattice site instead of the free volume at the pores. However, when an interstitial is located in Pore IV, all the three elements presented a less-stable structure than in other locations. This can be explained by the same bulk feature as described previously for Ag.

3.2 *Diffusivity of interstitials along grain boundaries*

In light of the strong segregation of FPs to GBs, which has been found for a typical grain diameter (0.8 μm) of SiC used in the TRISO application, we further investigate FB diffusion along the GB. Interstitials generally diffuse quickly inside the high-temperature reactor and can be obtained dramatically under irradiation condition. Therefore, we conducted simulation with respect to FP's introducing a single atom as an interstitial here.

As is shown in Table 1, a silver interstitial was found to be stable in Pore IIIL along ∑3 as compared with other locations. Therefore, the Ag atom was initiated at Pore IIIL. After several nanosecond simulations, the atom was found vibrating in Pore IIIL and could not overcome the energy barrier. However, the atom in Pore II was more active. In this simulation, Ag diffusion was found to be faster along the [01 $\bar{1}$] direction than along the [111] direction. This is due to the open channel along the [01 $\bar{1}$], which gives a possible pathway for the interstitial to migrate. The diffusion also undergoes directional reorientation. After 1 ns diffusion, the atom jumps along the [010] direction at 2000 K.

As stated in Equation 4, the diffusion coefficient contains two components, an intrinsic diffusion coefficient (meaning the diffusivity of the defect assuming it exists 100% of the time) and the concentration factor. Because Ag could only spend a fraction of the time as any specific defect type in the real case, the diffusion coefficient should be modified by the concentration ratio. The corresponding diffusion coefficients in the temperature range from 1200 to 3000 K, considering that the defect concentration ratio has been illustrated in Figure 2(a) as well as results from experiments[4], [7], [9], [10] and simulation [11].

The best-fit effective migration barrier and exponential pre-factor are summarized in Table 2. An estimation of the effective diffusion coefficient at 1873 K is 6.44×10^{-18} m^2/s. This value matches perfectly with the ion implantation result obtained by Leng et al. [7] and the *ab initio* calculation [11] in which the diffusion coefficients are 8.84×10^{-18} m^2/s at 1842 K and 3.69×10^{-18} m^2/s at 1873 K, respectively. The larger value, as compared with the bulk-diffusion prediction of 3.41×10^{-24} m^2/s at this temperature, for example, indicates the more important role that GB diffusion plays in Ag transport.

The close estimate to other ion implantation-based diffusion data in polycrystalline SiC also reinforces the accuracy of our MD prediction. However, a discrepancy still exists in comparison with the integral release results [9], [10]. While simulation and ion implantation can focus directly on a specific means of Ag transport through SiC, the integral release is independent of diffusion mechanisms. As the investigation in just ∑3 could be limited, the value falling below the measured data obtained in fuel studies may suggest other GBs may offer fast diffusion, or other effects, such as the presence of cracks, might play a significant role in silver diffusion.

Table 1. Defect formation energies associated with FPs in ∑3 as compared with the corresponding defects in bulk SiC.

Site						**Site**						**Site**					
	ABOP	Ab initio[11]	ABOP	ABOP	ABOP		ABOP	Ab initio[11]	ABOP	ABOP	ABOP		ABOP	Ab initio[11]	ABOP	ABOP	ABOP
Bulk	8.0909 [16]	7.39	3.7963 [16]	4.1101 [16]	7.8909 [16]	**Bulk**	5.9784 [16]	6.60	5.1762 [16]	4.1056 [16]	8.9955 [16]	**Bulk**	10.6170 [16]	10.49	7.5003 [16]	7.8279 [16]	18.2266 [16]
C1	6.4996	5.60	2.6798	4.9449	7.3548	**Si1**	4.0438	4.01	3.0646	3.1902	7.4886	**I**	8.9694	Unstable	5.8064	2.9458	15.5081
C2U	3.8915	3.63	2.4401	5.4145	5.7523	**Si2U**	5.2324	4.47	4.8753	4.0287	10.5293	**II**	6.3317	6.71	5.8656	4.1041	11.0984
C2L	5.0397	4.22	2.5095	2.1572	5.4576	**Si2L**	4.7115	4.74	4.0252	4.0678	9.1735	**IIa**	6.1417	4.70	5.4279	1.2019	11.0868
C3U	7.7733	4.59	3.8311	6.2413	6.6380	**Si3U**	5.2411	6.15	4.9384	5.7298	7.4956	**IIIL**	6.5524	5.99	7.1154	5.4693	13.6264
C3L	8.2916	4.76	4.0078	6.9392	7.0720	**Si3L**	4.7879	5.18	4.0144	3.9520	6.1763	**IIILa**	5.7695	3.27	5.1118	2.7589	12.7577
C4U	8.6339	4.99	2.6683	4.9319	7.1912	**Si4U**	5.4802	3.95	4.5930	3.3470	6.1547	**IVL**	9.5019	7.65	7.8447	8.4519	18.1299
C4L	9.0560	4.84	4.7138	6.9528	7.5539	**Si4L**	5.5318	3.69	4.5377	3.5890	6.5688	**IVLa**	9.1266	7.38	7.1388	8.4133	18.0255

Table 2. Effective migration energy and diffusion coefficient of FPs along as compared with values from experiments and simulations.

Element	**(eV)**				**(m^2/s)**			
	Bulk[16]	Exp.	*Ab initio*	Current	Bulk[16]	Exp.	*Ab initio*	Current
Ag	5.68	3.43[4]; 2.21[10]; 2.26[9]	3.95[11]	3.22	6.57	2.49[4]; 6.8[10]; 4.5[9]	1.71[11]	2.99
Pd	5.43		1.22	1.14	6.36			1.83
Ru	7.99			3.13	5.56			1.73
I	13.88			3.27	2.84			4.85

Palladium diffusion along GBs was also simulated in the same way as silver diffusion. As GBs have a comparatively more open structure than bulk due to relative misorientation of two adjacent grains contacting each other, Pd is thought to be able to freely migrate along GBs. The diffusion along ∑3 mainly exists along the [01$\bar{1}$] direction. The volume at Pore II is quite a bit larger than at other cores that provide open space for the interstitial to migrate. In consideration of the concentration ratio that resulted from the formation energy, the diffusion coefficient has been shown in Figure 2(b) in comparison with the *ab initio* calculation [30]. The diffusion coefficient is considerably higher than silver, which suggests that Pd can diffuse more readily along GBs than Ag.

The calculated atomic diffusion of Pd is much faster than the observed penetration rate of a palladium nodule [29]. This displays the slow dissolution and rapid regrowth of palladium nodules as possible ingress mechanism in addition to the suggested palladium nodules' migration along the GB. The effective migration energy and corresponding pre-factors are listed in Table 2. Moreover, the diffusion along ∑3 at 1500 K by MD calculations has well reproduced the *ab initio* calculations, which guarantees the reliability of the simulation we conducted here.

We continue to investigate Ru diffusion along this special CSL GB. Ru diffusion along ∑3 GB was found mainly in the <011> direction, which is prevalent in the observations for both Ag and Pd in earlier statements. Even though the lowest formation energy is identified at the C2L site, the jumps of the Ru atom can be noticeable once it overcomes the barrier from Core II to I. However, the diffusion is slower than that seen in the previous two elements, as indicated in the diffusion coefficient prediction demonstrated in Figure 2(c). The migration energy and diffusion pre-factor derived from the diffusivities are also summarized in Table 2. Because sparse diffusion-coefficient data have been published for Ru in SiC under pure thermal conditions, we found it to be of interest to exclude the defect-concentration ratio for the purpose of seeing the relationship between our simulation result and ion irradiation experiments because the interstitial can be generated uniformly with less impact on the formation energy than under thermal condition.

An estimation of the diffusion coefficient, without consideration of the defect-concentration ratio is 9.27×10^{-17} m^2/s at 1173 K. In experiments, Ru implanted SiC-PyC-SiC diffusion couples were irradiated with Si^{++} to 10 and 20 dpa at a temperature of 900°C at MIBL. The diffusivity extrapolated from SIMS was found to be 1.5×10^{-17} m^2/s and 5.5×10^{-17} m^2/s for 10 and 20 dpa, respectively, as indicated in Figure 3. The order of magnitude in the intrinsic diffusion coefficient of our simulation found a good match with the experimental data. Since interstitials can easily be obtained under irradiation conditions, the Ru diffusion as an interstitial could not be ignored.

Finally, iodine diffusion along GBs was tested. The migration along ∑3 can be three dimensional, which involves a zigzag path from Core II to Core I, in addition to a direct jump along the open channel of Core I. The occupation of an iodine interstitial at Core II can be either in plane or between planes. The corresponding traces of an iodine atom at 2200 K in Figure 4 clearly shows the preferable paths. This diffusion mechanism is accessible for all temperatures we investigated here. The effective diffusion coefficient in the range of 1200 to 3000 K are included in Figure 2(d), with the corresponding migration energy and diffusion pre-factor listing in Table 2. Our result suggests that iodine can diffuse faster along ∑3 than in bulk, where the effective migration energy along the GB also decreases dramatically.

The same set of experiments as used in the Ru case was also conducted using an iodine-implanted sample under irradiation condition. The slopes of the SIMS curve (Figure 5) for the prediction of grain boundary diffusivities at both 10 and 20 dpa, 8.3×10^{-17} m^2/s and 5.6×10^{-17} m^2/s, respectively, are somewhat larger than the estimated effective diffusivity in MD simulation at 900°C displayed in Figure 2(d). It is reasonable that the diffusion of iodine is accelerated due to ion irradiation where damages to the material could change the microstructure and create paths for iodine to diffuse; thus, it might be dangerous to make a direct comparison. However, it could be of interest to correlate the intrinsic diffusion coefficient of iodine to the irradiated condition. In such a correlation, less impact on the formation energy should be addressed than under thermal condition. This could help qualitatively understand the GB-boundary diffusion role in the presence of iodine.

The evaluated intrinsic diffusion coefficient in simulation at the experimental temperature shows a value of 2.21×10^{-16} m^2/s. This is, however, faster than what has been observed in the experiments. Iodine can react with SiC at relatively low temperature (200–300°C) to form tetraiodide (SiI4). It is suspected that the iodine may have formed SiI4, which would significantly limit the diffusion of iodine to the GB. Another observation of a decreased diffusion at 20 dpa, as compared with 10 dpa, may be explained by the same phenomenon. Even though limited results identify the dominant diffusion mechanism as more microstructure effect, and condition changes must be considered, calculations still show the evidence of preferable GB diffusion over bulk diffusion. This mechanism cannot be neglected once FPs are accessible at the GB.

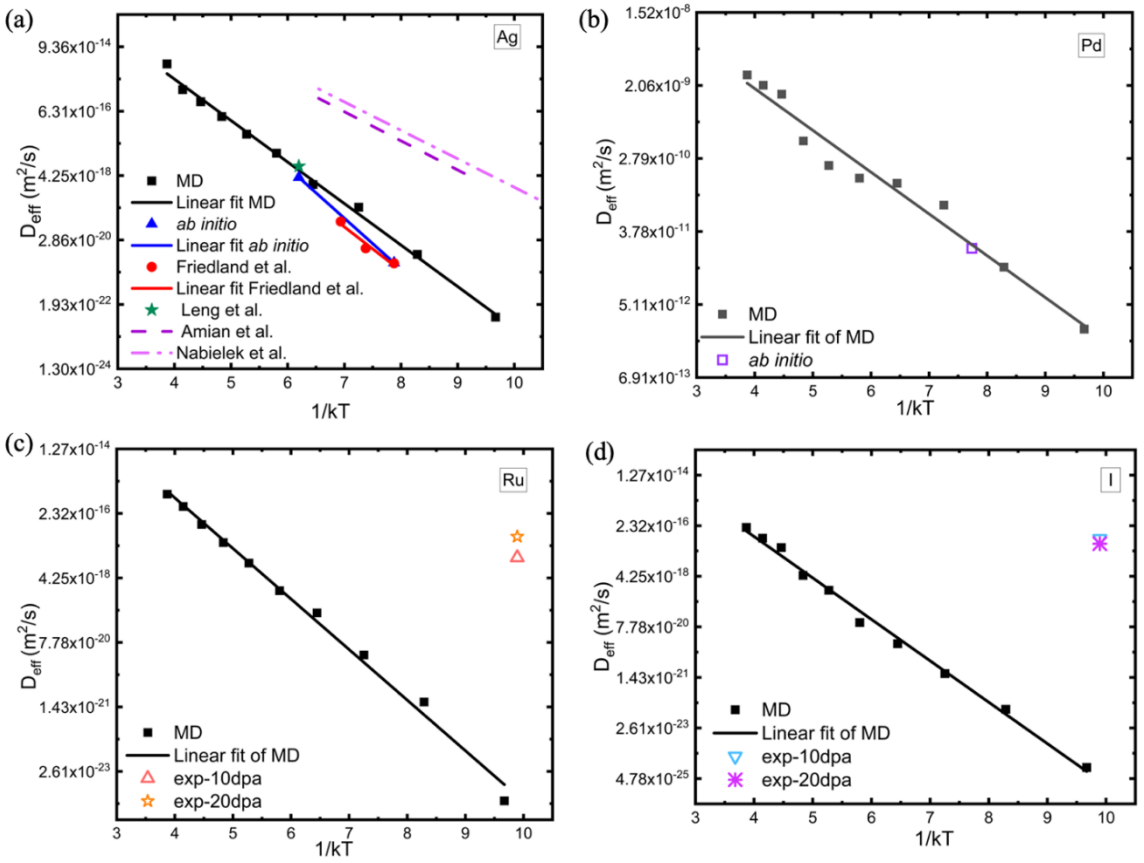

Figure 2. Effective diffusion coefficient of (a) Ag (Friedland et al. [4], Leng et al. [7], Nabielek et al. [10], Amian et al. [9], *ab initio*-Σ3 [11]); (b) Pd; (c) Ru; (d) I; along ∑3 as compared with computational and experimental results where available.

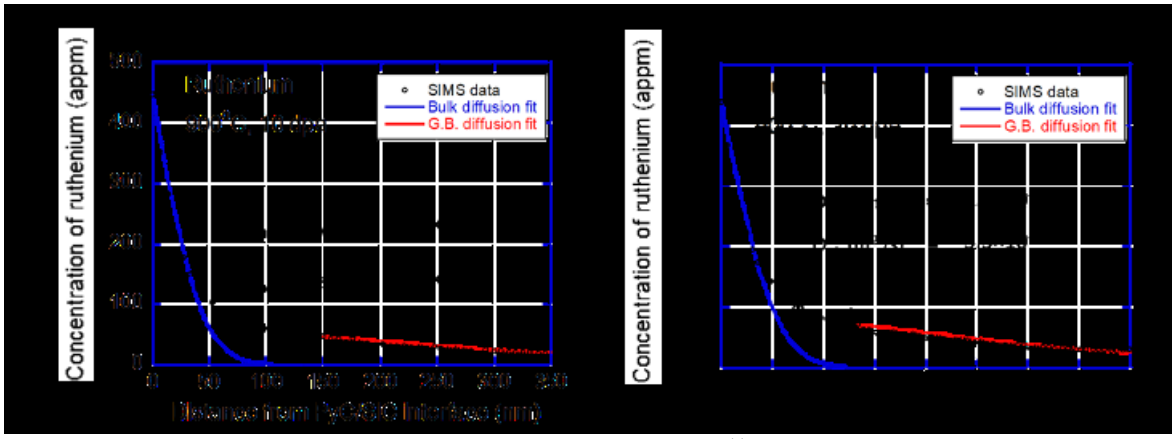

Figure 3. SIMS analysis of the ruthenium diffusivity in SiC after Si^{++} irradiation at 900°C to (a) 10 and (b) 20 dpa.

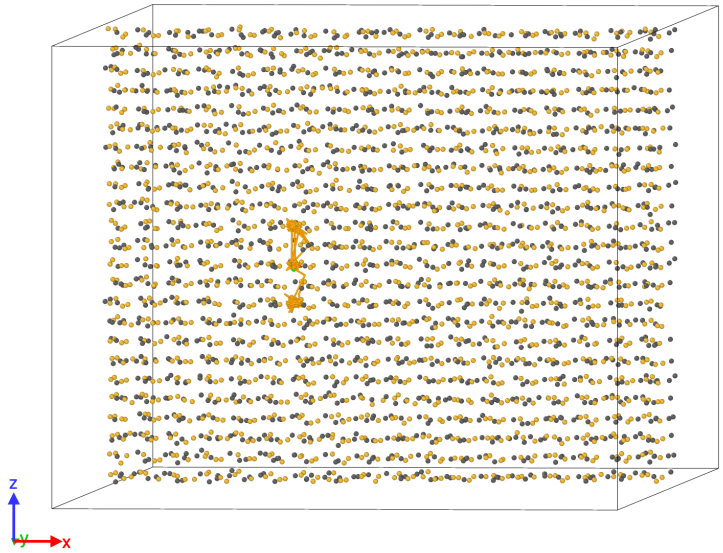

Figure 4. Diffusion trajectory of iodine along ∑3 at 1 ns, with the temperature of 2200 K (gray spheres stand for carbon, and yellow indicate silicon).

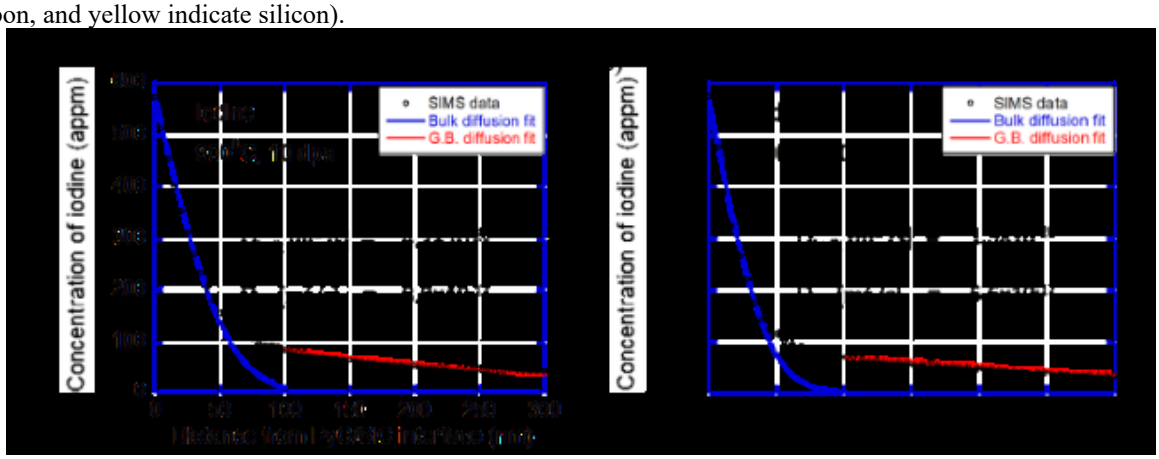

Figure 5. SIMS analysis of the iodine diffusivity in SiC after Si^{++} irradiation at 900°C to (a) 10 and (b) 20 dpa.

IV. CONCLUSION

In the present study, MD simulations were carried out to study four FP's transport, including Ag, Pd, Ru, and I at ∑3 GB, which forms the majority of the special CSL GBs in SiC within the TRISO fuel particle. We have determined the most stable structures of ∑3 and identified the possible locations that FPs can occupy. The general trend of decreasing in formation energy, as compared with bulk, indicates a strong segregation of FPs at GBs. It is also instructive to compare interstitial diffusion in the GBs to that in bulk. As segregation of FPs at the grain boundary is obvious, the energy required for those atoms to rest is relatively low as compared with those in bulk.

In addition to the direct comparison of migration energy and diffusion coefficient, it is without doubt that bulk diffusion is not a dominant mechanism. While GB diffusion can be orders of magnitudes faster than bulk diffusion, GB diffusion in FP transport is significant. This can be explained because GBs contain high concentrations of dislocations due to the relative misorientation between adjacent grains; therefore, they have a comparatively open structure. This results in diffusivities for GB transport that are much larger than analogous values for lattice diffusion. However, exception can be found as the complexity of microstructures of polycrystalline SiC could raise after neutron irradiation. The discrepancy between fuel studies and the simulated data for the silver case can itself be an evidence. The experiment measurements conducted at MIBL for the Ru- and I-implanted samples help elucidate both quantitatively and qualitatively the major role of GB diffusion in Ru, but its limited participation in I.

REFERENCES

[1] Y. Katoh, L. L. Snead, I. Szlufarska, and W. J. Weber, "Radiation effects in SiC for nuclear structural applications," *Current Opinion in Solid State and Materials Science*, vol. 16, no. 3. Elsevier Ltd, pp. 143–152, Jun. 01, 2012, doi: 10.1016/j.cossms.2012.03.005.

[2] S. D. Rubin, "TRISO-coated particle fuel phenomenon identification and ranking tables (PIRTS) for fission product transport due to manufacturing, operations and accidents." Accessed: Jun. 22, 2020. [Online]. Available: http://www.nrc.gov/reading-rm/doc-.

[3] B. P. Collin, D. A. Petti, P. A. Demkowicz, and J. T. Maki, "Comparison of silver, cesium, and strontium release predictions using PARFUME with results from the AGR-1 irradiation experiment," *J. Nucl. Mater.*, vol. 466, pp. 426–442, Nov. 2015, doi: 10.1016/j.jnucmat.2015.08.033.

[4] E. Friedland *et al.*, "Study of silver diffusion in silicon carbide," *J. Nucl. Mater.*, vol. 389, no. 2, pp. 326–331, May 2009, doi: 10.1016/J.JNUCMAT.2009.02.022.

[5] E. Friedland *et al.*, "Investigation of silver and iodine transport through silicon carbide layers prepared for nuclear fuel element cladding," *J. Nucl. Mater.*, vol. 410, no. 1–3, pp. 24–31, Mar. 2011, doi: 10.1016/J.JNUCMAT.2010.12.243.

[6] I. J. van Rooyen, T. M. Lillo, and Y. Q. Wu, "Identification of silver and palladium in irradiated TRISO coated particles of the AGR-1 experiment," *J. Nucl. Mater.*, vol. 446, no. 1–3, pp. 178–186, Mar. 2014, doi: 10.1016/J.JNUCMAT.2013.11.028.

[7] B. Leng *et al.*, "Effect of carbon ion irradiation on Ag diffusion in SiC," *J. Nucl. Mater.*, vol. 471, pp. 220–232, Apr. 2016, doi: 10.1016/J.JNUCMAT.2015.11.017.

[8] T. M. Lillo and I. J. van Rooyen, "Associations of Pd, U and Ag in the SiC layer of neutron-irradiated TRISO fuel," *J. Nucl. Mater.*, vol. 460, pp. 97–106, May 2015, doi: 10.1016/J.JNUCMAT.2015.02.010.

[9] W. Amian and D. Stöver, "Diffusion of Silver and Cesium in Silicon-Carbide Coatings of Fuel Particles for High-Temperature Gas-Cooled Reactors," *Nucl. Technol.*, vol. 61, no. 3, pp. 475–486, Jun. 1983, doi: 10.13182/NT61-475.

[10] H. Nabielek, P. E. Brown, and P. Offermann, "Silver Release from Coated Particle Fuel," *Nucl. Technol.*, vol. 35, no. 2, pp. 483–493, Sep. 1977, doi: 10.13182/NT35-483.

[11] S. Khalil, N. Swaminathan, D. Shrader, A. J. Heim, D. D. Morgan, and I. Szlufarska, "Diffusion of Ag along Σ 3 grain boundaries in 3C-SiC," *Phys. Rev. B*, vol. 84, no. 21, p. 214104, Dec. 2011, doi: 10.1103/PhysRevB.84.214104.

[12] D. Shrader *et al.*, "Ag diffusion in cubic silicon carbide," *J. Nucl. Mater.*, vol. 408, no. 3, pp. 257–271, Jan. 2011, doi: 10.1016/J.JNUCMAT.2010.10.088.

[13] J. Rabone and E. López-Honorato, "Density functional theory metadynamics of silver, caesium and palladium diffusion at β-SiC grain boundaries," *J. Nucl. Mater.*, vol. 458, pp. 56–63, Mar. 2015, doi: 10.1016/J.JNUCMAT.2014.11.032.

[14] N. Chen, Q. Peng, Z. Jiao, I. van Rooyen, W. F. Skerjanc, and F. Gao, "Ab initio study of the stability of intrinsic and extrinsic Ag point defects in 3CSiC," *J. Nucl. Mater.*, vol. 510, pp. 596–602, Nov. 2018, doi: 10.1016/J.JNUCMAT.2018.08.053.

[15] Q. Peng, N. Chen, Z. Jiao, I. J. van

Rooyen, W. F. Skerjanc, and F. Gao, "Reveal the fast and charge-insensitive lattice diffusion of silver in cubic silicon carbide via first-principles calculations," *Comput. Mater. Sci.*, vol. 170, p. 109190, Dec. 2019, doi: 10.1016/J.COMMATSCI.2019.109190.
[16] N. Chen, Q. Peng, Z. Jiao, I. van Rooyen, W. F. Skerjanc, and F. Gao, "Analytical bond-order potential for silver, palladium, ruthenium and iodine bulk diffusion in silicon carbide," *J. Phys. Condens. Matter*, vol. 32, no. 8, p. 085702, Feb. 2020, doi: 10.1088/1361-648X/ab5465.
[17] T. M. Lillo, I. J. van Rooyen, and J. A. Aguiar, "Silicon carbide grain boundary distributions, irradiation conditions, and silver retention in irradiated AGR-1 TRISO fuel particles," *Nucl. Eng. Des.*, vol. 329, pp. 46–52, Apr. 2018, doi: 10.1016/J.NUCENGDES.2017.11.048.
[18] R. Kirchhofer, J. D. Hunn, P. A. Demkowicz, J. I. Cole, and B. P. Gorman, "Microstructure of TRISO coated particles from the AGR-1 experiment: SiC grain size and grain boundary character," *J. Nucl. Mater.*, vol. 432, no. 1–3, pp. 127–134, Jan. 2013, doi: 10.1016/J.JNUCMAT.2012.08.052.
[19] S. Plimpton, "Fast Parallel Algorithms for Short-Range Molecular Dynamics," *J. Comput. Phys.*, vol. 117, no. 1, pp. 1–19, Mar. 1995, doi: 10.1006/JCPH.1995.1039.
[20] M. A. Tschopp and D. L. McDowell, "Structures and energies of Σ 3 asymmetric tilt grain boundaries in copper and aluminium," *Philos. Mag.*, vol. 87, no. 22, pp. 3147–3173, Aug. 2007, doi: 10.1080/14786430701255895.
[21] K. Tanaka and M. Kohyama, "Atomic and electronic structure analysis of Σ = 3 incoherent twin boundaries in β-SiC," *J. Electron Microsc. (Tokyo).*, vol. 51, no. suppl_1, pp. S265–S270, Mar. 2002, doi: 10.1093/JMICRO/51.SUPPLEMENT.S265.
[22] K. Tanaka and M. Kohyama, "Experimental and theoretical study of Σ = 3 incoherent twin boundary in β-SiC," *Philos. Mag. A Phys. Condens. Matter, Struct. Defects Mech. Prop.*, vol. 82, no. 2, pp. 215–229, 2002, doi: 10.1080/01418610208239595.
[23] P. Pirouz and J. Yang, "Anti-Site Bonds and the Structure of Interfaces in SiC," *MRS Proc.*, vol. 183, 1990, doi: 10.1557/proc-183-173.
[24] M. Kohyama and R. Yamamoto, "Tight-binding study of the {211} Σ=3 grain boundary in cubic silicon-carbide," in *Materials Research Society Symposium - Proceedings*, 1994, vol. 339, pp. 9–14, doi: 10.1557/proc-339-9.
[25] S. Dwaraknath and G. S. Was, "Development of a multi-layer diffusion couple to study fission product transport in β-SiC," *J. Nucl. Mater.*, vol. 444, no. 1–3, pp. 170–174, Jan. 2014, doi: 10.1016/J.JNUCMAT.2013.09.040.
[26] L. G. Harrison, "Influence of dislocations on diffusion kinetics in solids with particular reference to the alkali halides," *Trans. Faraday Soc.*, vol. 57, pp. 1191–1199, 1961, doi: 10.1039/TF9615701191.

[27] D. Gryaznov, J. Fleig, and J. Maier, "An improved procedure for determining grain boundary diffusion coefficients from averaged concentration profiles," *J. Appl. Phys.*, vol. 103, no. 6, 2008, doi: 10.1063/1.2887993.
[28] S. S. Dwaraknath and G. S. Was, "Radiation enhanced diffusion of cesium, strontium, and europium in silicon carbide," *J. Nucl. Mater.*, vol. 474, pp. 76–87, Jun. 2016, doi: 10.1016/j.jnucmat.2016.02.034.
[29] E. J. Olivier and J. H. Neethling, "Palladium transport in SiC," *Nucl. Eng. Des.*, vol. 244, pp. 25–33, Mar. 2012, doi: 10.1016/J.NUCENGDES.2011.12.018.
[30] J. Rabone, E. López-Honorato, and P. Van Uffelen, "Silver and Cesium Diffusion Dynamics at the β-SiC Σ5 Grain Boundary Investigated with Density Functional Theory Molecular Dynamics and Metadynamics," *J. Phys. Chem. A*, vol. 118, no. 5, pp. 915–926, Feb. 2014, doi: 10.1021/jp411156c.
[31] T.M.Lillo, I.J.van Rooyen, Influence of SiC grain boundary character on fission product transport in irradiated TRISO fuel, Journal of Nuclear Materials, Volume 473, May 2016, Pages 83-92